Proceedings World Geothermal Congress 2000
Kyushu - Tohoku, Japan, May 28 - June 10, 2000

DISSOLUTION, TRANSPORT AND PRECIPITATION OF SILICA IN GEOTHERMAL SYSTEM

Naoto Takeno[1], Tsuneo Ishido[1], and John W. Pritchett[2]
[1]Geological Survey of Japan, Tsukuba, Ibaraki 305-8567, Japan
[2]Maxwell Technologies Inc. San Diego, CA., USA

Key Words: reaction kinetics, silica, transport, numerical simulation

ABSTRACT

Dissolution and precipitation of silica polymorphs (amorphous silica, cristobalite and quartz) were incorporated into a geothermal reservoir simulator based on reaction kinetics. We simplified the reaction kinetics as silica minerals being always precipitated from or dissolved into the neutral dilute solution without a direct solid phase transition among them. Based on this assumption and published experimental data of rate constants and solubilities of silica minerals, three dimensional numerical simulations of geothermal system development were performed. Alteration zoning of silica minerals was reproduced in the simulations as observed in natural geothermal systems, and we examined the relation of the silica alteration zoning to the thermal and hydrological structure of the geothermal system.

1. INTRODUCTION

Silica minerals (quartz, cristobalite and amorphous silica) are common alteration minerals in geothermal systems. They form a one component system and dissolve congruently. Many data of solubility and dissolution/precipitation kinetics are published (Walther and Helgeson, 1977; Bohlmann et al., 1980; Rimstidt and Barnes, 1980; Fournier, 1982, 1983; Brady and Walther, 1990; Dove, 1994; Renders et al., 1995; Rimstidt, 1997). These characteristics of silica minerals are suitable for coupling chemical reaction with geothermal reservoir simulation in a reaction-transport system. Furthermore, understanding the behavior of silica minerals is useful to elucidate the development of the silica alteration zone as well as to estimate the influence of self-sealing or scaling by reinjection.

The studies on numerical simulation of the reaction-transport of silica involve one dimensional (Walder and Nur, 1984; Lowell et al., 1993) and two dimensional (Yano, 1994) flow models with silica in equilibrium with quartz. It also involves a one dimensional flow model with amorphous silica reaction kinetics (Malate and O'Sullivan, 1992), a one dimensional flow model with quartz and amorphous silica reaction kinetics (Rimstidt and Barnes, 1980; Wells and Ghiorso, 1991), and a two dimensional flow model with quartz or amorphous silica reaction kinetics (Cathles, 1983; White, 1997). Takeno et al. (1998a and b) tried to incorporate dissolution/precipitation kinetics of silica minerals, quartz, cristobalite and amorphous silica in a geothermal reservoir simulator RIGHTS and applied this simulator to geothermal system in a two dimensional model. In the two dimensional models, silica transport was assessed in flow-lines "across" a vertically high permeability zone (Takeno et al., 1998b). In this study, we will complete the assessment, in three dimensional models, for flow-lines "along" a vertically high permeability zone and "across" it, as well as examine the relation of silica alteration zones to the thermal and hydrological structure of the geothermal system.

In geothermal systems, many polymorphs of silica minerals are observed, such as quartz, α-cristobalite, β-cristobalite, α-tridymite, and β-tridymite (Kimbara, 1977). In this study, we will treat dissolution and precipitation of three common silica polymorphs, namely α-quartz, α-cristobalite, and amorphous silica (hereafter simply called quartz, cristobalite, and amorphous-silica, respectively). We neglect direct solid-solid phase transition among the minerals. Although biomineralization of silica minerals in some hot springs (Akabane et al., 1997; Tazaki, 1995) and the influence of salinity and pH on silica mineral solubility (Fourinier, 1983) as well as on precipitation/dissolution kinetics (Dove, 1994; Bohlmann et al., 1980) are known, for simplicity we neglect these effects and assume a neutral dilute solution. We also neglect dissolution of other minerals such as feldspar. Plagioclase has a higher dissolution rate than quartz so that its effect on aqueous silica transport is important. We think that this should be treated in future assessments.

2. GOVERNING EQUATIONS

The basic governing equations used in this simulation are mass balance, momentum balance, and energy conservation. Chemical reactions are implemented as add-on packages that are independent of the physical parameters. Governing equations for physical parameters are solved first, followed by the equations for chemical reactions and silica mass transport. Dissolution or precipitation of silica minerals gives feedback to the change of porosity, permeability, and reaction surface area. The governing equations for physical parameters of the next step are then solved. Calculations are performed at each step in this way.

Dissolution and precipitation rate for the *i*th silica mineral is given as follows. The left side is positive for dissolution and negative for precipitation.

$$\frac{\partial m_{H_4SiO_4}}{\partial t} = k_{+i}\frac{A_i}{M}\left(1-\frac{Q}{K_i}\right) \tag{1}$$

where

$$Q = m_{H_4SiO_4} \tag{2}$$

m is the molality of aqueous silica species (in this study, only H_4SiO_4 is considered), t is the time, k_{+i} is the dissolution rate constant of *i*th silica mineral, A_i is the reaction surface area of *i*th silica mineral, M is the mass of solution, and K_i is the solubility constant of *i*th silica mineral. Activities of silica

minerals and water are assumed as unity, and the activity coefficient of H_4SiO_4(aq) is assumed as unity. Solubility constants K_i are calculated as follows:

Quartz (Rimstidt, 1997)

$$\log K = -0.0254 - 1107.12/T \quad (3)$$

α-cristobalite (Rimstidt and Barnes, 1980)

$$\log K = -0.0321 - 988.2/T \quad (4)$$

Amorphous silica (Rimstidt and Barnes, 1980)

$$\log K = 0.3380 - 7.889\times10^{-4}T - 840.1/T \quad (5)$$

T is absolute temperature. Rate constants k_{+i} are given by Rimstidt and Barnes (1980). We used a rate constant for quartz recalculated from the data revised by Rimstidt (1997):

$$\log k_{+(qtz)} = -0.7324 - 3705.12/T \quad (6)$$

$$\log k_{+(\alpha-crist)} = -0.739 - 3586/T \quad (7)$$

$$\log k_{+(am.silica)} = -0.369 - 7.890\times10^{-4}T - 3438/T \quad (8)$$

T is absolute temperature. We neglected pressure effects for these constants and regarded them to be the same as on the vapor-liquid saturation curve. Many empirical or theoretical functions of grain size or porosity are known for permeability (Domenico and Schwartz, 1990). We used the following equation derived from Kozeny-Carman relation:

$$\frac{current\_permeability}{initial\_permeability} = \left(\frac{current\_prosity}{initial\_porosity}\right)^3 \quad (9)$$

We also assumed the following relationship between porosity and total reaction surface area.

$$\frac{current\_area}{initial\_area} = \left(\frac{current\_porosity}{initial\_porosity}\right)^{0.5} \quad (10)$$

In this study, we followed the reaction surface area model used in Takeno et al. (1998b). The principles of this model are as follows. 1) Primary minerals, when undersaturated, in rock dissolve into solution. 2) Secondary minerals, when oversaturated, precipitate only in pore spaces from the solution, cover the pore wall and redissolve into the solution when undersaturated. For precipitation, the total surface area A is partitioned into A_i in proportion to the precipitation rate of ith silica mineral. 3) The deposition of secondary minerals on pore walls inhibits the dissolution of primary minerals in the rock. However, we consider that perfect blocking of soluble minerals in the rock by trace amounts of insoluble precipitates is not realistic due to the roughness of the pore surface.

For this reason, we introduced a parameter F^* ($0<F^*<<1$) and we virtually subdivided the total surface area into surface area of precipitated secondary silica minerals A_p and surface area of rock A_f which is composed of primary silica minerals and inert minerals. Then following equations are imposed.

$$F = \frac{V_p}{F^*(V_p + V_l)} \quad (11)$$

$$G = \frac{A_f}{A} \quad (12)$$

so that

$$A_f = GA \quad (13)$$

$$A_p = (1-G)A \quad (14)$$

$$G = (1-F)^2 \quad \text{for } F<1$$
$$= 0 \quad \text{for } F \geq 1 \quad (15)$$

V_p is the volume occupied by secondary silica, and V_l is the volume occupied by liquid. For the dissolution of secondary silica minerals, A_i is given from A_p by volume-weighting among the silica minerals. For the dissolution of primary silica minerals, A_i is given from A_f by volume-weighting among the silica and inert minerals. The simulation code RIGHTS solves the above equations by the finite difference method. In this simulation, we treat discontinuous phenomenon such as appearance and disappearance of minerals so that we cannot use a large time step. In this regard, there is no advantage for using the implicit method, so we use the explicit method for solving the equations.

3. GEOTHERMAL MODEL-BOUNDARY CONDITION AND INITIAL CONDITION

We examined a three dimensional porous cube of 2 km x 2 km x 2 km which is uniformly subdivided into 20 computational grids in each axis. These computational grids build four blocks A to D (Figure 1). The rock properties of these blocks are shown in Table 1. The common rock properties for all four blocks are density (2500 kg/m^3), heat capacity (1000 J/kg/deg), and thermal conductivity (2 W/m/deg). All boundaries (bottom, top, left, right, back, and front) are insulated. The bottom, left, right, back, and front boundaries are impermeable. A top layer is open to free pure water at 10^{O}C and 1 bar. Heat source of (i, j, 1) grid hss_{ij1} W/m^3 within a bottom layer is given as follows.

$$hss_{ij1} = 20\times10^{-5}\left(1 - \sqrt{(100i)^2 + (100j)^2}\,/\,2000\right)(350 - t)$$

if $hss_{ij1}<0$, $hss_{ij1}=0$ (16)

Heat sinks for so called "radiative/convective condition" were given as 0.08x(t-10) W/m^3 within top layer grids. t is the temperature in centigrade. Thermal equilibrium between rock and fluid was always assumed. All blocks consist of rock containing 20 weight% quartz (the other part is inert) with pores filled with pure water at 10^{O}C in the initial state. From the preliminary simulation, the results were not sensitive to the variation of F^*, because only the most insoluble mineral,

quartz, was included in the rock as a primary mineral. Therefore, *F** is fixed as 0.01 for all cases. Simulation was carried out for up to 50,000 years. In all experiments, block A is a highly permeable vertical zone assumed as a high angle fracture zone. In the experiment 11/0 to 11-2, the block B, C, and D are given the same rock properties to represent homogeneous formation of varying permeability penetrated by vertical high permeable zone. In the experiment 11-4 and 11-5, a cap rock of low permeability (1e-17m^2) is placed in the different positions, at the top or shallow part of a low permeable aquifer (1e-16 m^2) respectively. The experiment 11-3 and 11-9 uses the same model as the experiment 11-4 and 11-5 except a high permeable aquifer (1e-15 m^2). The experiment 11-7, 11-5, and 11-8 uses the same model as the experiment 11-5 except a heat source power within the bottom layer. The heat sources of 11-7 and 11-8 are doubled and halved from 11-5, respectively.

4. RESULTS AND DISCUSSION

The results show that an amorphous silica zone appears at and around the surface where fluid is discharge from a vertical high permeable block A, and that this zone overlaps with cristobalite. These zones correspond to subsurface up-flow. Secondary quartz is concentrated along the upflow zone in a mushroom shaped pattern. Primary quartz in the rock was dissolved from the bottom, and silica is transported along the upflow path to the top. These results correspond well with the occurrence of a silica alteration zone in a natural geothermal system.

The detail of the zoning pattern is different among the experiments. From the experiments 11-0 to 11-2 (Figure 2), we can evaluate the influence of permeability of the blocks neighboring the block A. With more permeable blocks, the amorphous silica zone and cristobalite zone are widened, their maximum density become higher and the thermal energy of the whole system decreases. This indicates that silica and thermal energy are transported effectively up to the surface in high permeable blocks.

The experimental results 11-4 and 11-5 (Figure 3 upper-left) show that the position of a cap rock in the low permeability reservoir is not sensitive to the thermal energy, distribution of silica zones, and maximum density of silica polymorphs. The experimental results 11-3 and 11-9 (Figure 3 lower-left) show that the cristobalite zone is widened in the higher permeability block B, but other parameters do not show significant difference. By comparing the low permeability 11-4/11-5 and high permeability 11-3/11-9 experiments, it is noted that the amorphous silica zone and cristobalite zone of the latter are greater in area and density than the former, but significant difference in thermal energy and quartz zone cannot be observed. Therefore, it can be deduced that high permeability aquifer facilitates transport of heat and silica which results to decrease of thermal energy and wide silica alteration zone. The amorphous silica and cristobalite zones are more sensitive to aquifer permeability than thermal energy.

Experimental results 11-7, 11-5, and 11-8 (Figure 3 right) show that high powered heat source promote high thermal energy and wide silica alteration zone. Halved heat source (11-8) does not produce an amorphous silica zone. Therefore, silica alteration zone is also dependent on the thermal input of the geothermal system. Takeno et al. (1998b) suggested that cristobalite zone disappears below 100^{O}C from their simulation and it conforms to cristobalite disappearance below 100^{O}C in active geothermal fields (Hayashi, 1973; Browne, 1978; Kimbara and Ohkubo, 1978). This tendency is also recognized as a disappearance temperature of the cristobalite zone below 100^{O}C to 150^{O}C in this study. However, the grid is too large to evaluate it precisely and further assessment is needed.

5. CONCLUSIONS

From the numerical reservoir simulation incorporating silica dissolution/precipitation kinetics, we showed that amorphous silica zone and cristobalite zone develop along vertically high permeability zone (i.e. fracture zone) and it is dependent on aquifer permeability and thermal input. High thermal input favors the development of an amorphous silica zone and a cristobalite zone, as well as high total thermal energy. High aquifer permeability without cap rock favors transport of silica, development of silica alteration zones, and removal of thermal energy. Cap rock impedes removal of thermal energy to cause insensitivity of total thermal energy to aquifer permeability, but silica alteration zones are still sensitive to aquifer permeability.

REFERENCES

Akabane, H., Yasuda, I., Miyajima, H., Goto, K., Honoki, H. (1997). Precipitation of silica sinter in hot spring water*. *Jour. Geol. Soc. Japan*, Vol. 103 (2), pp.154-162.

Bohlmann, E. G., Mesmer, R. E. and Berlinski, P. (1980). Kinetics of silica deposition from simulated geothermal brines. *Soc. Petrol. Engineers Jour.*, Vol. 20 (4), pp.239-248.

Brady, P. V. and Walther, J. V. (1990). Kinetics of quartz dissolution at low temperatures. *Chem. Geol.*, Vol. 82 (3/4), pp.253-264.

Browne, P. R. L. (1978). Hydrothermal alteration in active geothermal fields. *Ann. Rev. Earth Planet. Sci.*, Vol. 6, pp.229-250.

Cathles, L. M. (1983). An analysis of the hydrothermal system responsible for massive sulfide deposition in the Hokuroku basin of Japan. *Econ. Geol. Monograph*, Vol. 5, pp.439-487.

Domenico, P. A. and Schwartz, W. F. (1990). *Physical and Chemical Hydrogeology*, 824p., John Wiley& Sons, New York, p.76.

Dove, P. M. (1994). The dissolution kinetics of quartz in sodium chloride solutions at 25^O to 300^{O}C, *Am. Jour. Sci.*, Vol. 294 (6), pp.665-712.

Fournier, R. O. (1982). An equation correlating the solubility of quartz in water from 25^O to 900^{O}C at pressures up to 10,000 bars. *Geochim. Cosmochim. Acta*, Vol. 46 (10), pp.1969-1973.

Fournier, R. O. (1983). A method of calculating quartz solubilities in aqueous sodium chloride solutions. *Geochim. Cosmochim. Acta*, Vol. 47 (3), pp.579-586.

Hayashi, M. (1973). Hydrothermal alteration in the Otake geothermal area, Kyushu*. *Jour. Japan Geotherm. Energy Assoc.*, 10 (3), pp.9-46.

Kimbara, K. (1977). Some cristobalites and tridymites in geothermal area*. *Jour. Japan Geotherm. Energy Assoc.*, Vol. 14 (1), pp.13-20.

Kimbara, K. and Ohkubo, T. (1978). Hydrothermal altered rocks found in an exploration bore-hole (No. SA-1), Satsunan geothermal area, Japan*. *J. Assoc. Petrol. Mineral. Econ.*, Vol. 73 (5), pp.125-136.

Lowell, R. P., Cappellen, P. V. and Germanovich, L. N. (1993). Silica precipitation in fractures and the evolution of permeability in hydrothermal upflow zones. *Science*, Vol. 260, pp.192-194.

Malate, R. C. M. and O'Sullivan, M. J. (1992). Mathematical modeling of silica deposition in a porous medium. *Geothermics*, Vol. 21 (3), pp.377-400.

Renders, P. J. N., Gammons, C. H. and Barnes, H. L. (1995). Precipitation and dissolution rate constants for cristobalite from 150 to 300^{O}C. *Geochim. Cosmochim. Acta*, Vol. 59 (1), pp.77-85.

Rimstidt, J. D. (1997). Quartz solubility at low temperatures. *Geochim. Cosmochim. Acta*, Vol. 61 (13), pp.2553-2558.

Rimstidt, J. D. and Barnes, H. L. (1980). The kinetics of silica-water reactions. *Geochim. Cosmochim. Acta*, Vol. 44 (11), pp.1683-1699.

Takeno, N., Ishido, T. and Pritchett, J. W. (1998a). Numerical simulation of development of silica alteration zoning in geothermal system-preliminary study based on kinetic reaction-transport model*. *Jour. Min. Soc. Japan*, Vol. 27 (3), pp.157-166.

Takeno, N., Ishido, T. and Pritchett, J. W. (1998b). Alteration zonation of silica minerals in a geothermal system - a numerical simulation based on reaction-transport model. In: *Proceedings 20th New Zealand Geothermal Workshop*, pp.259-264.

Tazaki, K. (1995). Electron microscopic observation of biomineralization in biomats from hot springs*. *Jour. Geol. Soc. Japan*, Vol. 101 (4), pp.304-314.

Walder, J. and Nur, A. (1984). Porosity reduction and crustal pore pressure development. *Jour. Geophys. Res.*, Vol. 89 (B13), pp.11539-11548.

Walther, J. V. and Helgeson, H. C. (1977). Calculation of the thermodynamic properties of aqueous silica and the solubility of quartz and its polymorphs at high pressures and temperatures. *Am. Jour. Sci.*, Vol. 277 (10), pp.1315-1351.

Wells, J. T. and Ghiorso, M. R. (1991). Coupled fluid flow and reaction in mid-ocean ridge hydrothermal systems: the behavior of silica. *Geochim. Cosmochim. Acta*, Vol. 55 (9), pp.2467-2481.

White, S. P. (1997). Modeling the dissolution and precipitation of quartz in a deep geothermal system. In: *Proceedings 19th New Zealand Geothermal Workshop*, pp.93-98.

Yano, Y. (1994). Permeability change in the evolution of hydrothermal convection system due to silica dissolution/precipitation** (abstract). *Jour. Geotherm. Res. Soc. Japan*, Vol. 16 (2), p.218.

*in Japanese with English abstract
**in Japanese

Table 1. Rock properties of the unit and heat source. Rock properties of each unit are shown as porosity/permeability (isotropic)m^2/ reaction surface area m^2/m^3 separated by '/'. Arrows indicates that an item is the same as its left.

run	block A	block B	block C	block D	heat source
11-0	0.05/1e-14/10	0.05/5e-15/100	→	→	eq.(16)
11-1	0.05/1e-14/10	0.05/1e-16/100	→	→	eq.(16)
11-2	0.05/1e-14/10	0.05/1e-15/100	→	→	eq.(16)
11-3	0.05/1e-14/10	0.01/1e-17/10	0.05/1e-15/100	→	eq.(16)
11-4	0.05/1e-14/10	0.01/1e-17/10	0.05/1e-16/100	→	eq.(16)
11-5	0.05/1e-14/10	0.05/1e-16/100	0.01/1e-17/10	0.05/1e-16/100	eq.(16)
11-7	(all blocks same	as 11-5		)	2 x eq.(16)
11-8	(all blocks same	as 11-5		)	0.5 x eq.(16)
11-9	0.05/1e-14/10	0.05/1e-15/100	0.01/1e-17/10	0.05/1e-15/100	eq.(16)

Table 2. Summary of the experimental results. Total thermal energy of the geothermal system (J), and maximum density (kg/m^3) of the silica minerals after 50,000 years.

run	thermal energy	amorphous silica	cristobalite	quartz
11-0	1.1E+18	0.065	1.7	26
11-1	2.1E+18	0.0019	0.11	16
11-2	1.7E+18	0.016	0.37	21
11-3	2.0E+18	0.0078	0.18	17
11-4	2.1E+18	0.0014	0.10	16
11-5	2.1E+18	0.0015	0.10	16
11-7	2.4E+18	0.0090	0.19	22
11-8	1.8E+18	0	0.04	9.9
11-9	2.1E+18	0.0073	0.21	16

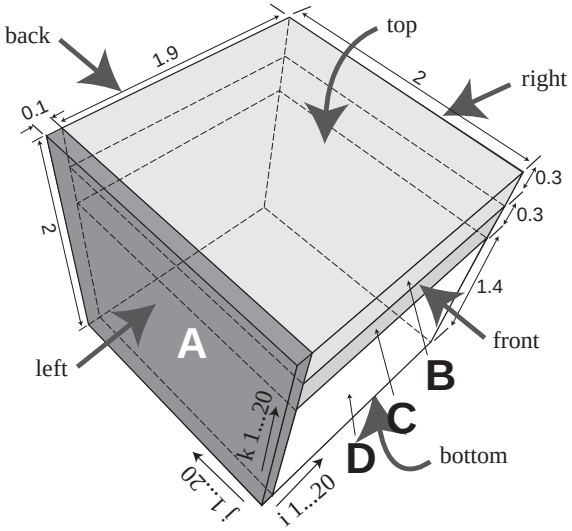

Figure 1. Geometry and structure of the model for numerical simulation. unit in km.

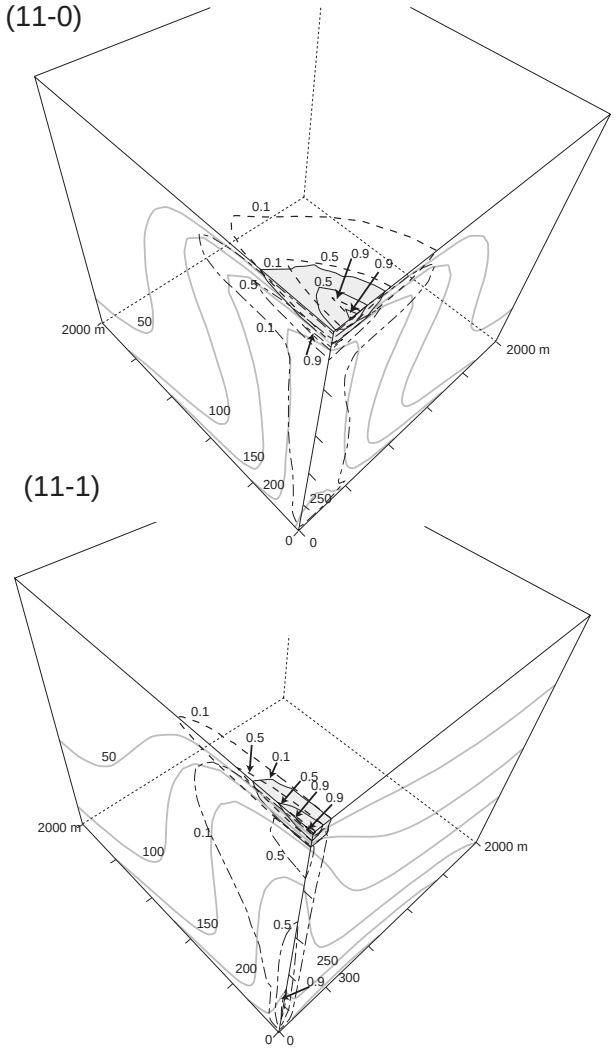

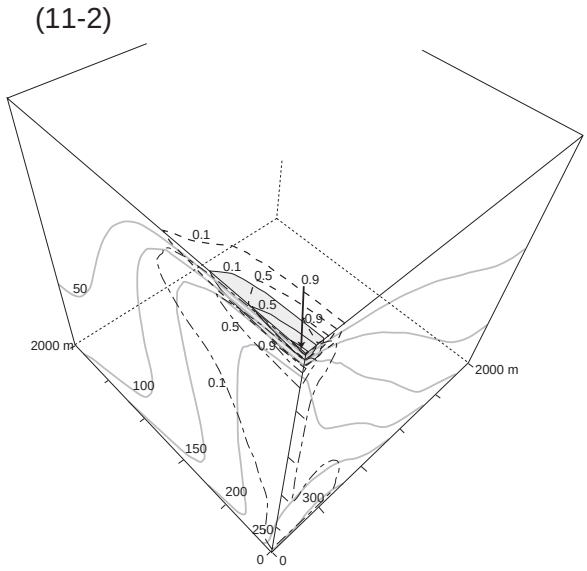

Figure 2. Experimental result of run 11-0 to 11-1. Thin line: amorphous silica, broken line: cristobalite, chain line: quartz, number indicates fraction of the maximum density of each mineral. Shaded area indicates amorphous silica more than 0.1 of its maximum density. Thick line: temperature (C).

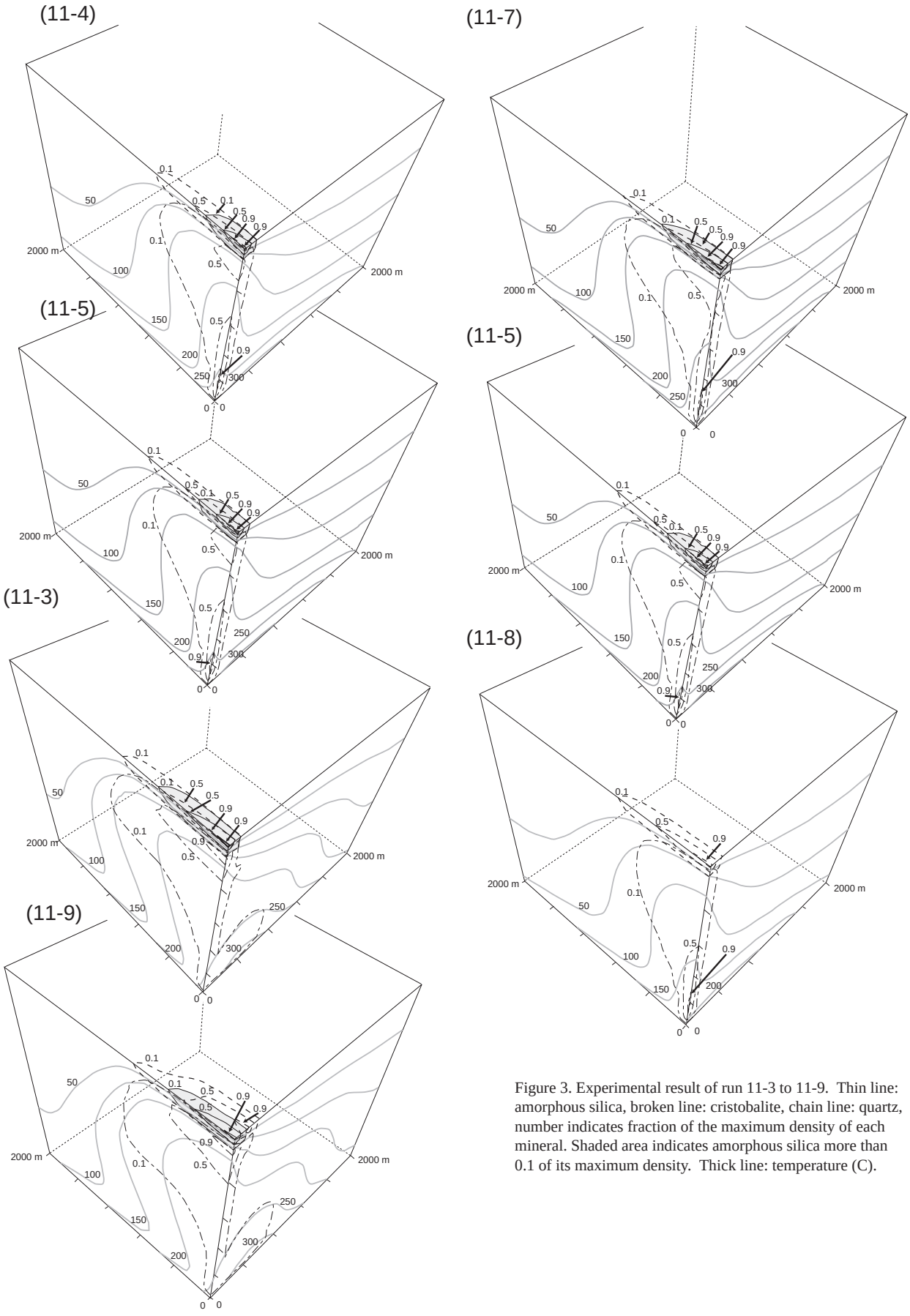

Figure 3. Experimental result of run 11-3 to 11-9. Thin line: amorphous silica, broken line: cristobalite, chain line: quartz, number indicates fraction of the maximum density of each mineral. Shaded area indicates amorphous silica more than 0.1 of its maximum density. Thick line: temperature (C).